Effectiveness of Nonpeptide Clinical Inhibitor TMC-114 on HIV-1 Protease with Highly Drug Resistant Mutations D30N, I50V, and L90M

Andrey Yu. Kovalevsky,[†] Yunfeng Tie,[‡] Fengling Liu,[†] Peter I. Boross,[†,§] Yuan-Fang Wang,[†] Sofiya Leshchenko,[∥] Arun K. Ghosh,[∥] Robert W. Harrison,[⊥] and Irene T. Weber*[,†,‡]

Department of Biology and Department of Chemistry, Molecular Basis of Disease, and Department of Computer Science, Georgia State University, Atlanta, Georgia 30303, Department of Biochemistry and Molecular Biology, Faculty of Medicine, University of Debrecen, Debrecen, Hungary, and Department of Chemistry and Medicinal Chemistry, Purdue University, West Lafayette, Indiana 47907

Received September 21, 2005

The potent new antiviral inhibitor TMC-114 (UIC-94017) of HIV-1 protease (PR) has been studied with three PR variants containing single mutations D30N, I50V, and L90M, which provide resistance to the major clinical inhibitors. The inhibition constants (K_i) of TMC-114 for mutants PR_{D30N}, PR_{I50V}, and PR_{L90M} were 30-, 9-, and 0.14-fold, respectively, relative to wild-type PR. The molecular basis for the inhibition was analyzed using high-resolution (1.22−1.45 Å) crystal structures of PR mutant complexes with TMC-114. In PR_{D30N}, the inhibitor has a water-mediated interaction with the side chain of Asn30 rather than the direct interaction observed in PR, which is consistent with the relative inhibition. Similarly, in PR_{I50V} the inhibitor loses favorable hydrophobic interactions with the side chain of Val50. TMC-114 has additional van der Waals contacts in PR_{L90M} structure compared to the PR structure, leading to a tighter binding of the inhibitor. The observed changes in PR structure and activity are discussed in relation to the potential for development of resistant mutants on exposure to TMC-114.

Introduction

HIV-1 protease (PR)[a] is an attractive target for antiretroviral therapy, since it plays an integral role in the virion maturation by processing Gag and Pol polyproteins into the structural proteins and enzymes. Hence, the inhibition of the PR produces noninfectious viral particles. HIV PR inhibitors (PIs) were developed in 1995 and now are a major component of the AIDS chemotherapy called highly active antiretroviral therapy (HAART),[1,2] which includes administering PIs together with reverse transcriptase inhibitors. This drug regimen has dramatically improved the survival of patients and converted AIDS into a treatable medical condition.

Currently, there are around 20 FDA-approved drugs for the treatment of HIV infection and many others are in development.[3] Among these, seven are PIs: amprenavir (and fosamprenavir), atazanavir, indinavir, lopinavir, nelfinavir, ritonavir, and saquinavir.[4] These drugs are considered the most effective drugs currently available for the treatment of AIDS.[5,6] Despite the tremendous success the PIs have had in improving lives of infected people, side effects[7] and the emergence of drug resistant (and cross-resistant)[8,9] PR mutants pose great challenges in treating HIV.

The most disturbing development in the battle against the HIV infection has been the appearance of mutations that confer resistance to all available PIs in clinical use. The drug molecules were designed to optimize the fit to the PR binding site. As soon as a mutation changes the shape of the cavity, the drug significantly loses its inhibiting potency. Therefore, new therapeutic agents are always necessary. The new drugs must exhibit low susceptibility to resistant mutations and ideally show fewer side effects than the existing treatments.[10]

TMC-114 is a next-generation nonpeptidic PI that is extremely potent against multidrug resistant strains, with IC_{50} values of 3−29 nM for the inhibition of the PR mutants selected for resistance to saquinavir, indinavir, nelfinavir, or ritonavir,[11,12] and is also highly active against different HIV subtypes.[13] TMC-114 is now in phase III clinical trials and shows superiority to the approved clinical PIs.[14] TMC-114 is a chemical analogue of amprenavir, with the terminal tetrahydrofuran (THF) moiety being fused to another THF group to form a novel bis-THF substituent. TMC-114 was designed to introduce more polar interactions with main chain atoms of PR. Our crystallographic analysis has confirmed that the design goal was met by new hydrogen-bond interactions of TMC-114 with Asp 29 and 30 of PR.[11,15] However, TMC-114 has shown lower inhibition of the mutants selected for resistance to amprenavir than for other mutants.[11]

TMC-114 was observed to bind to the PR with very favorable change in enthalpy ($\Delta H = -12.1$ kcal/mol),[16] whereas ΔH is small or even negative for indinavir, nelfinavir, and saquinavir.[17,18] On the other hand, the change in entropy ($T\Delta S$) upon binding for most of the PIs in clinical use compensates for the lack of the favorable ΔH. Therefore, the binding energy of the PIs (ΔG) comes mostly from a substantial increase in entropy of the solvent being expelled from the active site cavity by an incoming PI. This suggests that most PIs have very few attractive interactions when bound to the PR, and changes in the geometry of the cavity due to mutations in the binding site can result in considerable loss of the PI's affinity to the PR. An enlarged binding site cavity has been observed for PR containing mutations I84V and I54V, which introduce smaller amino acids.[15,19] However, compensating conformational changes have

* Corresponding author. Phone: 404-651-0098. Fax: 404-651-2509. E-mail: iweber@gsu.edu.
[†] Department of Biology, Molecular Basis of Disease, Georgia State University.
[‡] Department of Chemistry, Molecular Basis of Disease, Georgia State University.
[§] University of Debrecen.
[∥] Purdue University.
[⊥] Department of Computer Science, Georgia State University.

[a] Abbreviations: PR, protease; HIV-1, human immunodeficiency virus type 1; HAART, highly active antiretroviral therapy; AIDS, acquired immunodeficiency syndrome; PI, protease inhibitor; THF, tetrahydrofuran.

10.1021/jm050943c CCC: $33.50 © 2006 American Chemical Society
Published on Web 02/02/2006

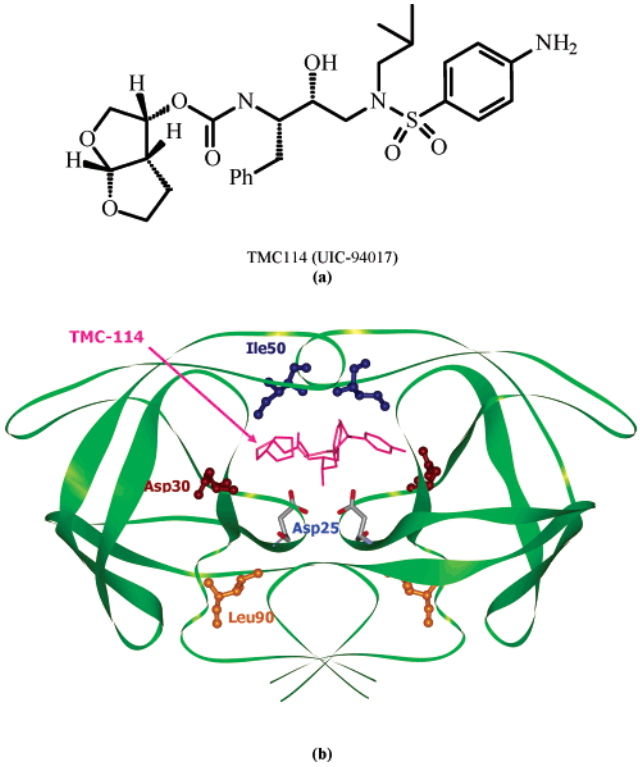

Figure 1. (a) Molecular diagram of the TMC114 inhibitor. (b) PR dimer structure (green ribbons). The sites of mutation are indicated using ball-and-stick representation for Asp30, Ile50, and Leu90. Catalytic aspartate residues are shown in a stick representation. Only one subunit is labeled.

been observed in the crystallographic analysis of inhibitor-complexed PR with active site mutations[15] and nonactive site mutations.[20]

To understand the molecular basis for the potency of TMC-114, it is crucial to obtain high-resolution crystal structures of various complexed PR mutants. Such structures are also beneficial in predicting which active site mutations may generate resistant HIV. Previously, we have reported the crystal structures of TMC-114 in complex with the PR mutants V82A and I84V.[15] These two mutant complexes showed small structural changes compared to PR, consistent with the K_i values being similar to those of PR. Now we have selected three more mutations for analysis, D30N, I50V, and L90M, which confer high levels of resistance in clinical isolates.[21] The inhibitor and location of the mutations in PR dimer are shown in Figure 1. D30N was chosen because this mutation was expected to alter the hydrogen-bond interaction of Asp 30 side chain with the aniline NH2 group of TMC-114. D30N is a major mutation almost exclusively selected for resistance to nelfinavir.[22] The aspartate-to-asparagine substitution eliminates the negative charge of aspartate without significantly changing the geometry of the side chain. PR_{D30N} showed a variation in activity for the hydrolysis of peptides representing different Gag and Gag-Pol cleavage sites while its stability is retained compared to the wild-type PR.[23] For example, CA-p2 peptide was cleaved 4−5 times more efficiently than $p6^{pol}$-PR and PR-RT. Crystal structures of PR_{D30N} complexed with substrate analogues corresponding to CA-p2 and p2-NC cleavage sites revealed distinct changes in the position of the Asn30/Asn30′ side chains when the mutant structures are compared to each other or to the wild-type structures, consistent with the observed variable specificity.[24] Mutation I50V was selected for study since it is the primary mutation that emerges during treatment with amprenavir,[25] the drug that is chemically most similar to TMC-114. The mutation reduces the size of the hydrophobic side chain by one methyl group and is expected to increase the size of the binding cavity and reduce the affinity for inhibitor. Mutation L90M was chosen because it is associated with resistance to all known PIs currently in clinical use. It was found to be a major mutation selected on exposure to saquinavir or nelfinavir in combination with G48V and D30N mutations, respectively.[26] L90M mutation is located outside the inhibitor binding site but is proximal to the catalytic triad Asp25-Thr26-Gly27.

Here, we describe the inhibition data and crystal structures of TMC-114 with mutants PR_{D30N}, PR_{I50V}, and PR_{L90M}. These structures are compared with our reported structures of TMC-114 with PR, PR_{V82A}, and PR_{I84V}.[15] The structural analysis demonstrated overall similarity of the three structures and the wild type protease. Only when the I50V mutation is introduced do the protein−inhibitor interactions significantly change. A number of attractive interactions between the side chain of Ile50 and the aromatic carbons of the TMC-114's aniline group are lost in the PR_{I50V} structure.

Results

Kinetic Data for Mutants. The kinetic data were measured for PR (henceforth corresponds to wild-type protease) and a set of five mutants (PR_{D30N}, PR_{I50V}, PR_{V82A}, PR_{I84V}, PR_{L90M}) using a microplate fluorescence assay, and the parameters are listed in Table 1. The six mutants varied in their activity on the fluorescent substrate relative to PR. The k_{cat} value varied from 0.2 to 7.6 min^{-1}, while the K_m showed little change (26−57 μM). PR_{V82A} was similar to PR in the k_{cat}/K_m value, while PR_{I84V} and PR_{I50V} had 65% and 38% of the PR value. PR_{D30N} had dramatically lower k_{cat}/K_m of 10% of the PR value. In contrast, PR_{L90M} had more than 2-fold increased k_{cat}/K_m.

The mutants varied in the inhibition by TMC-114, with K_i values ranging from 0.14- to 30-fold of the PR value. The relative order of inhibition was $PR_{L90M} \gg PR > PR_{V82A} > PR_{I84V} > PR_{I50V} > PR_{D30N}$. Indinavir showed a different relative order of inhibition of the mutants using the same fluorescent spectroscopic assay: $PR \approx PR_{L90M} > PR_{V82A} > PR_{I84V} > PR_{D30N} > PR_{I50V}$. The relative K_i values for TMC-114 and indinavir were similar for PR_{V82A} and PR_{I84V}. TMC-114 was 3-fold worse than indinavir for inhibition of PR_{D30N}, a mutation most common on treatment with nelfinavir. However, indinavir had 2−10-fold higher relative inhibition than TMC-114 for PR_{I50V} and PR_{L90M}, consistent with the potency of TMC-114 on HIV strains resistant to indinavir. Interestingly, TMC-114 is more effective than indinavir on PR_{I50V}, despite the common occurrence of this mutation on exposure to amprenavir, which is chemically most similar to TMC-114.

Crystal Structures. The crystal structures of drug resistant mutants PR_{D30N}, PR_{I50V}, and PR_{L90M} have been determined in complex with TMC-114. Crystallographic statistics are summarized in Table 2. The crystallographic asymmetric units contain a PR dimer with the residues in two subunits labeled 1−99 and 1′−99′. The three complexes crystallized in the same space group ($P2_12_12$) and diffracted to the near-atomic resolutions of 1.22−1.45 Å. The structures were refined with anisotropic *B*-factors, solvent molecules, and hydrogen atoms, giving the final *R*-factors in the range of 13.0−15.2%. There was clear electron density for all atoms of the protease, the inhibitor, and solvent molecules in all the structures. The representative electron density is shown in Figure 2. The inhibitor adopts an extended conformation with two alternate orientations in the active site cavity with almost equal occupan-

Table 1. Kinetic Parameters from the Fluorescence Assay for Hydrolysis of Peptide Ac-RE(Edans)SQNY[a]PIVRK(Dabcyl)R-CO-NH_2 and Inhibition by TMC-114 or Indinavir (IDV) of PR, PR_{D30N}, PR_{I50V}, PR_{V82A}, PR_{I84V}, and PR_{L90M}

protease	K_m, μM	k_{cat}, min^{-1}	k_{cat}/K_m, $min^{-1}\,nM^{-1}$	K_i, nM (relative) TMC-114	K_i, nM (relative) IDV
PR	36 ± 8	2.7 ± 0.5	75 ± 20	0.22 ± 0.05 (1)	0.6 ± 0.1 (1)
PR_{D30N}	31 ± 5	0.21 ± 0.02	7 ± 1	6.6 ± 1.0 (30)	7.0 ± 1.0 (12)
PR_{I50V}	57 ± 12	1.7 ± 0.2	30 ± 7	2.0 ± 0.4 (9)	10.4 ± 1.0 (17)
PR_{V82A}	26 ± 2	2.4 ± 0.1	92 ± 8	0.8 ± 0.06 (3.6)	1.34 ± 0.12 (2.2)
PR_{I84V}	39 ± 7	2.0 ± 0.2	50 ± 10	1.1 ± 0.2 (5)	2.51 ± 0.35 (4.2)
PR_{L90M}	38 ± 5	7.6 ± 0.7	200 ± 34	0.030 ± 0.004 (0.14)	0.8 ± 0.1 (1.33)

[a] The cleaved peptide bond.

Table 2. Crystallographic Data for PR_{D30N}, PR_{I50V}, and PR_{L90M} in Complex with TMC-114

	PR_{D30N}	PR_{I50V}	PR_{L90M}
space group	$P2_12_12$	$P2_12_12$	$P2_12_12$
unit cell dimensions (Å)			
a	58.49	58.70	58.26
b	86.13	85.79	85.91
c	45.94	46.15	46.05
resolution range (Å)	50−1.45	50−1.22	50−1.25
unique reflections	40644	64113	62487
R_{merge} (%) overall (final shell)	8.9 (57.5)	9.0 (40.2)	5.9 (59.6)
data range for refinement (Å)	10−1.45	10−1.22	10−1.25
R_1 ($I > 2\sigma(I)$)	13.4	11.7	13.2
R_{work} (%)	15.2	13.0	14.1
R_{free} (%)	21.8	18.8	18.9
no. of solvent (total occupancies)	178.0	171.1	185.5
completeness (%) overall (final shell)	98.0 (86.0)	91.9 (53.3)	96.4 (82.6)
rms deviation from ideality (Å)			
bonds	0.011	0.014	0.015
angle distance	0.034	0.037	0.040
average *B*-factors (Å^2)			
main chain	16.2	15.4	18.4
side chain	22.7	19.9	23.7
inhibitor	12.9	12.9	14.4
solvent	33.4	28.8	34.9
occupancies for alternate conf of TMC-114 (%)	52/48	60/40	51/49

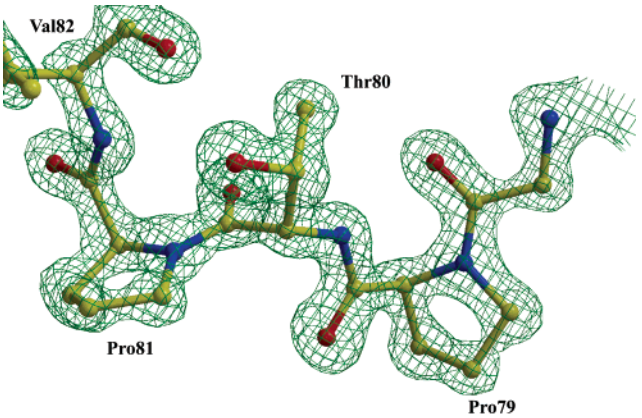

Figure 2. $2F_o - F_c$ electron density map for residues Pro79-Thr80-Pro81 of PR_{I50V} complex. The contour level is 2.6σ.

cies related by a 180° rotation. The average *B*-factors were low for protein and inhibitor atoms. The highest resolution structure of PR_{I50V} had the lowest *R*-factor and showed the lowest *B*-factors for the protein and inhibitor atoms.

Alternate conformations were modeled for residues in all the crystal structures. In each case there was a clear electron density for both positions of the side chains, as shown by the examples in Figure 3. There were 18 alternate conformations modeled for PR_{D30N}, 29 for PR_{L90M}, and 30 for PR_{I50V}. Interestingly, for PR_{D30N}, the average *B*-factors are as low as for the PR_{I50V} structure, even though the latter was modeled with more

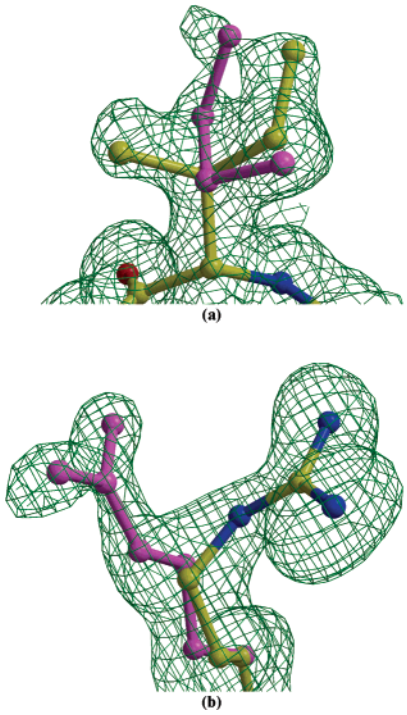

Figure 3. Alternate side-chain positions of PR_{I50V} structure shown in the $2F_o - F_c$ map. The residues drawn are Ile84 (62/38% occupancies) (a) and Arg57 (66/34% occupancies) (b). The electron density map is contoured at a level of 1.6σ (a) and 1.1σ (b). The major conformations are colored by atom type, and the minor conformations are in pink.

Table 3. Comparison of Residues with Alternate Conformations for PR, PR_{D30N}, PR_{I50V}, PR_{V82A}, PR_{I84V}, and PR_{L90M} in Complex with TMC-114[a]

residue	PR	PR_{D30N}	PR_{I50V}	PR_{V82A}	PR_{I84V}	PR_{L90M}
Lys7	AB	AB	B	A	AB	B
Glu21	AB	AB	AB	B	AB	AB
Asp/Asn30	AB	B	AB	A	AB	AB
Ser37	AB	AB	AB	A	A	A
Met46	AB	B	AB	AB	AB	AB
Glu65	AB	A	B	AB	AB	A
Ile/Val84	AB	B	AB	A	B	AB
Leu97	AB	AB	AB	A	AB	B

[a] Only the residues that have alternate conformations in at least one protease subunit are listed.

alternate conformations. Generally, the alternate conformations were observed for the side chains on the surface of the protein, especially for the residues with long side chains, such as glutamate, glutamine, lysine, and arginine. Table 3 compares the residues that have alternate conformations in structures with TMC-114, including those previously determined.[15] Eight residues, Lys7, Glu21, Asp/Asn30, Ser37, Met46, Glu65, Ile/Val84, and Leu97, have alternate conformations in at least one subunit in all structures. In five structures, the main-chain atoms

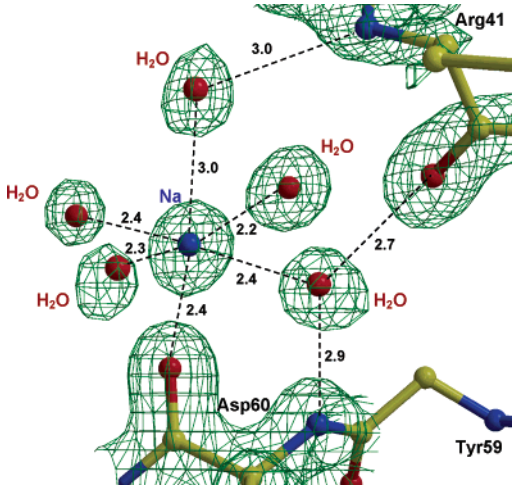

Figure 4. $2F_o - F_c$ electron density map for the sodium cation region in the PR_{L90M} structure. The map is contoured at the 2.0σ level. The sodium atom has a distorted square bipyramidal coordination of water and carbonyl oxygen atoms. The short contacts in the Na^+ coordination sphere and hydrogen bonds are indicated by dashed lines, with the interatomic distances in Å. The side-chain of Tyr59 is omitted for clarity.

of Ile/Val50 and 50′ in the two subunits, located at the tips of the flaps, have two alternate conformations, with relative occupancies of about 60/40%. The carbonyl groups can flip about 180° while hydrogen-bond interactions are maintained with the amide nitrogens at the tip of the other flap.

Similar to the previous structures with TMC-114 inhibitor,[15] the high resolution of the diffraction data for the structures studied here allowed modeling of two shells of solvent. The solvent was modeled with more than 200 water molecules, ions, and other small molecules from the crystallization solutions; many of these small molecules have partial occupancies. The ions modeled were sodium, chloride, and sulfate, while glycerol was refined in the PR_{L90M} structure. The example of $2F_o - F_c$ electron density for the sodium cation region in PR_{L90M} structure is shown in Figure 4. The average *B*-factors for the solvent atoms were 28.8 Å^2 for PR_{I50V}, 33.4 Å^2 for PR_{D30N}, and 34.9 Å^2 for PR_{L90M}.

Comparison of Inhibitor−Protease Interactions. A. Hydrogen-Bond Network. The TMC-114 inhibitor has been designed to optimize the number of hydrogen-bond interactions with the protease, especially those with the main-chain atoms, to have a better affinity for the protein and withstand drug-resistant mutations.[11] In the three structures studied here, the hydrogen-bond interactions of the inhibitor with the corresponding mutant protease are similar to those in the PR. As an example, the network of hydrogen bonds is shown in Figure 5 for PR_{L90M}. The central hydroxymethyl isostere has strong H-bond interactions with the two aspartic acid carboxylate groups that mimic the tetrahedral transition state−protease interactions. One water-mediated contact is found for PR_{D30N}, PR_{I50V}, and PR_{L90M} that involves the tetrahedrally coordinated water linking the SO_2 and carbonyl of the urethane moiety with the main-chain amides of residues 50 and 50′. This water is conserved in almost all structures of the PR with inhibitors, substrates, and substrate analogues, except for the structures with the inhibitors designed explicitly to substitute this H_2O (DMP323,[27,28] DMP450[29]). Although the water molecule is symmetrically connected to the amide atoms of residues 50 and 50′, it has very close (2.3−2.4 Å) (values are given for the distances between heavy atoms) and strong interaction with one sulfonamide oxygen and a long and therefore weaker hydrogen

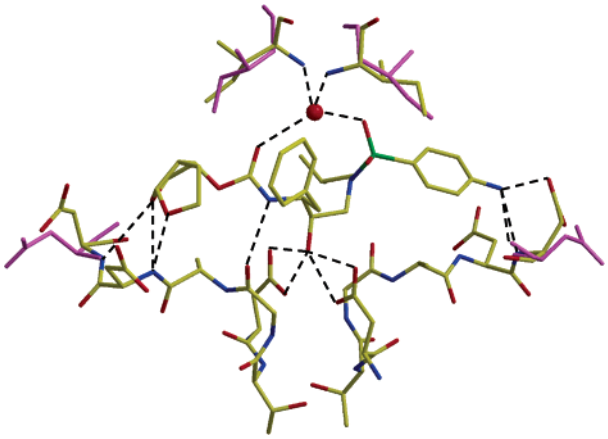

Figure 5. The hydrogen-bond network between the inhibitor and the protease in the PR_{L90M} structure. Residues 30, 30′, 50, and 50′ have two alternate conformations including main-chain atoms, and the minor conformations are colored in pink.

bond with the urethane's carbonyl (3.0−3.1 Å) in all the structures. In addition, the amide nitrogen of the urethane part forms a weak hydrogen bond to the main-chain carbonyl of Gly27 or Gly27′ for the second inhibitor orientation. The distance of 3.1−3.2 Å is similar in the wild type and the mutant structures.

The terminal groups of the TMC-114 bear hydrogen-bond donor (aniline) and acceptor (bis-THF) moieties. Due to the presence of two inhibitor orientations, these groups occupy almost the same sites and interact with the main-chain and side-chain atoms of Asp29, Asp30, Asp29′, and Asp30′ (Asn30 and Asn30′ in the case of PR_{D30N}). Asp/Asn30 show alternate conformations with occupancies ∼50/50% in the six structures with TMC-114 mentioned in the paper that are probably related to the alternate conformations of the inhibitor (no alternate conformations were modeled for Asp30 in the structures by King et al.[16]). Residue 30 is one of only two amino acids (the other is 84) located in the inhibitor binding cavity that have alternate conformations in the six structures (Table 3). In PR_{D30N} and PR_{L90M} structures, bis-THF oxygens have H-bonds to the amide nitrogen atoms of residues 29 and 30 (and 29′, 30′ for the other subunit) with distances of ∼2.9−3.3 Å. The longer distances of 3.1−3.4 Å are observed with residue 30 in the I50V mutant structure. The *p*-NH_2 substituent of the aniline moiety interacts closely with residue 30 or 30′, including contacts with both main- and side-chain atoms. The amino group makes similar hydrogen bonds to the carboxyl group, amide nitrogen, and carbonyl oxygen in the wild type and the mutant structures. Differences are observed in PR_{D30N} and PR_{I50V} structures. In PR_{D30N}, the aniline group has water-mediated contacts to the side chain of Asn30 or to one of the alternate conformations of Asn30′ (Figure 6). Such water-mediated contacts with both residues 30 and 30′ are not present in the other structures. In PR_{I50V}, a very strong H-bond (2.5 Å) to the carboxylate of Asp30 prevents the formation of other H-bonds with the main-chain amide and carbonyl of the same residue; while for the other subunit the interactions with the main chain of Asp30′ are similar to those of the other structures (Figure 7).

B. C−H···O Interactions. There are a number of other attractive interactions that are of importance for the strong binding of the inhibitor in the PR active site cavity. These are termed C−H···O contacts.[30] Several such interactions have been observed in every structure with TMC-114. The sulfonamide oxygen atoms have close contacts of 2.8−2.9 Å with the C_α atoms of Gly49 in one inhibitor orientation and with Gly49′

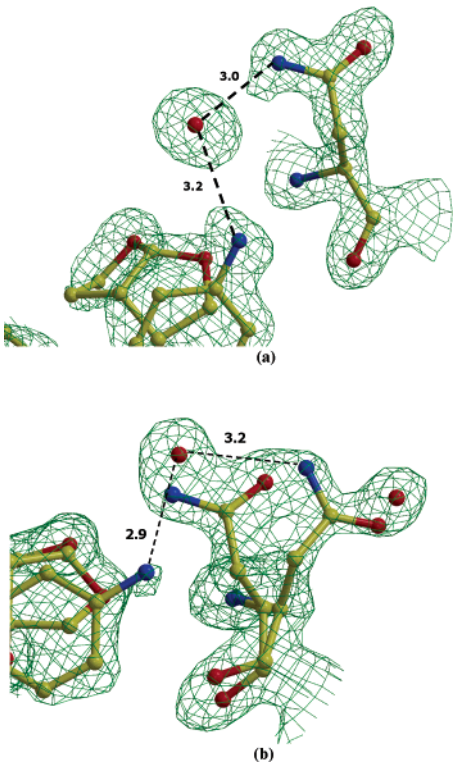

Figure 6. $2F_o - F_c$ electron density maps for residues Asn30 (a) and Asn30′ (b) of PR_{D30N}. The maps clearly show the two alternate conformations of Asn30′ (56/44% occupancies) and water-mediated contacts to the aniline moiety of TMC114. The contour level is 1.6σ. Interactions of bis-THF moiety are not shown.

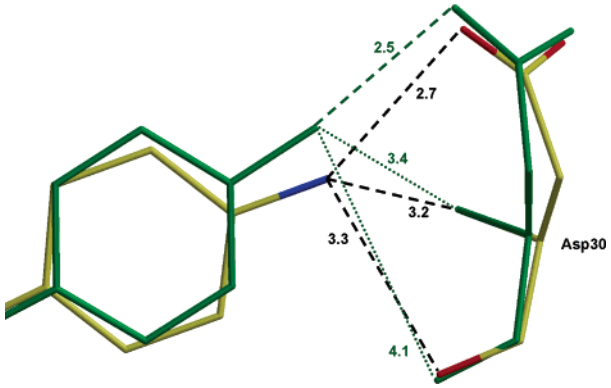

Figure 7. Interactions of the aniline group of TMC114 with residue Asp30 in PR and PR_{I50V} structures. PR is colored by the atom type, and PR_{I50V} is shown as green sticks. The alternate conformation of the Asp30 side chain in PR and the second orientation of the inhibitor for both structures are omitted for clarity. The interactions of the other inhibitor orientation with residue Asp30′ of the other protease subunit are similar in all the structures.

for the alternate inhibitor orientation. These C−H···O contacts are conserved in all the structures mentioned here. In addition, the sulfonamide oxygen atoms make close but weaker contacts with the terminal CH_3 groups of Ile50 or Ile50′ (~3.1 Å). It has to be emphasized that in the PR_{I50V} mutant structure, these interactions with the SO_2 moiety are not possible for Val50. On the other hand, Val50′ is oriented differently, and two symmetric interactions of 2.8 Å are observed between its methyl groups and each of the sulfonamide oxygen atoms (Figure 8). The former contacts involving the α-carbon of Gly49 and 49′ are stronger and therefore more stabilizing, since the C_α is activated by the electron-withdrawing atoms connected to it. In contrast, the latter CH_3···O interactions have less stabilizing

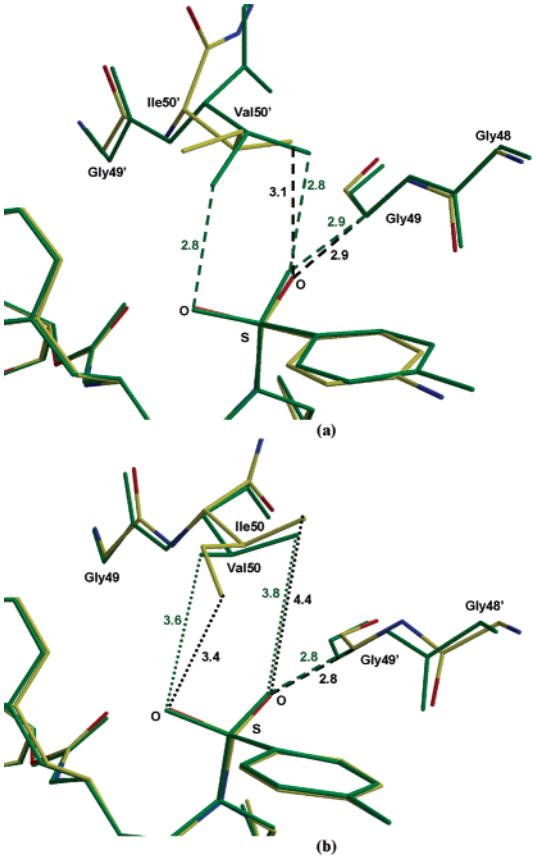

Figure 8. C-H···O interactions between the sulfonamide moiety of TMC114 and the protease atoms. PR is colored by the atom type, and PR_{I50V} is shown as green sticks. The alternate conformation of Ile50′ in PR_{WT} and Val50′ in PR_{I50V} and the second orientation of the inhibitor for both structures are omitted for clarity. The alternate conformations of residue 50′ that do not make C−H···O interactions with TMC114 are omitted. Parts a and b show the contacts with the residues in different subunits of PR. For the other structures these contacts are similar to those of PR.

effect and are less important. Even weaker interactions are found between the oxygen atoms of the sulfonamide moiety and terminal CH_3 groups of Ile84 or Ile84′. The distances are in the range from 3.2 to 3.7 Å; the longest distances are for the PR structure and the shortest distances are for PR_{I50V} and PR_{L90M}. The loss of these interactions in the PR_{I84V} structure may contribute to the severalfold increase in the K_i value for TMC-114 inhibitor. The bis-THF group forms one C−H···O interaction with the carbonyl oxygen of Gly48, or Gly48′ in the other inhibitor orientation. This interaction is conserved and has similar distances of 2.8−3.0 Å in the structures.

Although the C−H···O interactions are weaker stabilizing contacts compared to the N−H···O and N−H···N hydrogen bonds mentioned above, their significance cannot be overestimated. Since some of the interactions are made with the main-chain atoms of the protein, they play a valuable role in the ability of TMC-114 to effectively inhibit various protease mutants.

C. Hydrophobic Interactions. The hydrophobic interactions include the van der Waals contacts of H···H and H···π nature. The first type of interaction can be realized between closely oriented alkyl groups or an alkyl group and aromatic group when the hydrogen atom an alkyl group is located almost in the plane of the aromatic ring. The second category includes contacts formed when an alkyl group's hydrogen atom is positioned on top of an aromatic ring but not necessarily facing the ring's center.

Bis-THF, aniline, and the central phenyl group are the primary substituents involved in the hydrophobic interactions with the protease atoms. P1 (Ph) and P1′ (*t*-Bu) groups have van der Waals interactions with residues Leu23, Gly49, Ile/Val50, Pro81, Val82, and Ile84 from both subunits of PR. The CG atom of Pro81′ in PR has close H···H interactions (carbon···carbon distance is ∼3.6Å) with the P1 phenyl ring of the inhibitor. These interactions are similar in other structures and involve also Pro81 when the residue has a single conformation for the side chain at CG atom. Moreover, in PR_{I50V} the interaction involving Pro81 is even shorter, the distance is ∼3.3 Å, and Pro81 is fully ordered. Such close contacts between hydrogen atoms are repulsive and should contribute a destabilizing component to the overall binding energy of TMC-114. Therefore, in the PR_{I50V} structure the inhibitor binding must be destabilized even further compared to the other structures.

The π-system of the inhibitor's aniline moiety forms a number of C−H···π interactions with the side-chain atoms of residues Ala28, Val32, Ile47, and Ile/Val50 from both PR subunits. Unlike the H···H contacts, the interactions with the aromatic π-system are not just van der Waals contacts but have some electrostatic character and therefore are more favorable. Ile47 and Ile47′ have weak interactions with the aniline benzene ring in the range of 4.1−4.5 Å in the PR and the mutant structures. The side-chain atoms of Ile50, Ile50′ and Ala28, Ala28′ have stronger contacts to both conformations of the inhibitor. The distances are comparable in most of the structures studied (3.6−3.9 Å). One alternate conformation of Ile50 in PR_{L90M} structure makes 3.3−3.4 Å long contacts with the π-system of aniline, which perhaps become destabilizing at such short distances. The shortening of these interactions in the L90M mutant can probably be attributed to the longer chain of methionine pushing the active site aspartate side chains toward the inhibitor (see in more detail below). In PR_{I84V} the side chain of Ile50 is fully ordered; however, similar short contacts are formed. In PR_{V82A}, TMC-114 has a single orientation in the crystal; only the terminal aniline group occupies two alternate sites. Interestingly, in this structure the side chain of Ile50′ makes only van der Waals contacts to the π-system of aniline moiety, the closest being 4.0 Å long. The mutation of Ile50 to Val50 results in these contacts being longer and therefore weaker, or lost completely, for Val50′ or Val50, respectively, in the PR_{I50V} structure (Figure 9). Remarkably, the C−H···π interactions formed with residues Val32 or Val32′ are significantly shorter than those with Ala28, Ile47, or Ile/Val50. The distances are 3.3−3.4 Å in all the structures with TMC-114. The inhibitor···Val32 interactions cannot be ignored on the grounds of the occurrence of alternate conformations in residue 32, as it has single conformation in PR_{D30N} and PR_{V82A} structures for both subunits of the protease.

D. Structural Differences between the Mutants and the Wild-Type PR. Five protease−inhibitor structures in the current series were obtained in the same space group, $P2_12_12$, while the PR_{V82A} was the only structure crystallized with TMC-114 in the space group $P2_12_12_1$. The former structures are very similar, with the rms deviations not exceeding 0.1 Å for the main-chain atoms computed with respect to the PR. The PR_{V82A} structure showed larger rms differences compared to the wild-type PR of 0.35 Å, owing to differences in lattice contacts in the two space groups. Differences of more than 1 Å are observed for the main-chain atoms of residues 37−40, 37′−48′, and 54′−56′. However, these large differences reflect variations in positions of residues on the surface of the protein that are not involved in interactions with the inhibitor. There was a small

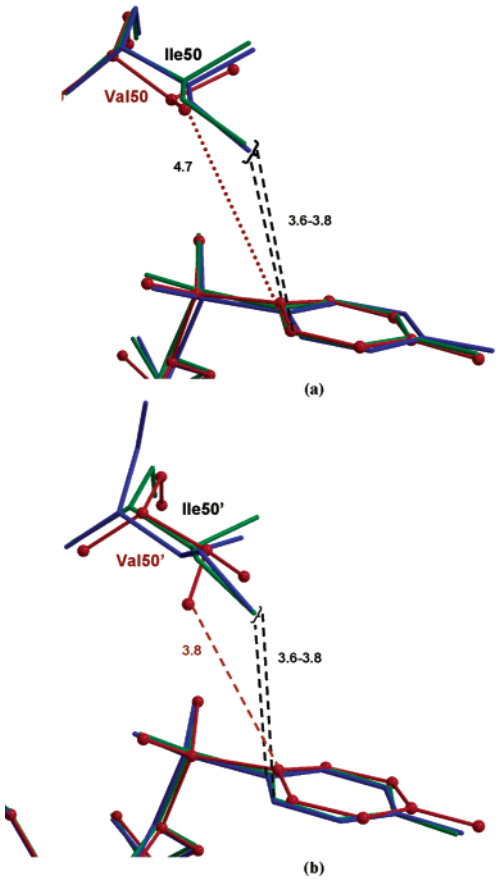

Figure 9. C−H···π interactions between the side chains of Ile50 or Val50 (a) and Ile50′ or Val50′ (b) with the aromatic ring of TMC114's aniline moiety in PR_{D30N} (blue), PR_{I50V} (red ball-and-stick representation), and PR_{L90M} (green). Alternate conformations of residue 50 that do not form close contacts to the aromatic ring are omitted for clarity.

movement of main-chain atoms of residue 50′ in PR_{I50V} toward TMC-114, which partly compensated for the change from isoleucine in PR to the smaller valine side chain. This conclusion is supported by the presence of a 3.8 Å long contact made by a methyl group of Val50′ and a carbon of the aniline moiety. Alternatively, the main chain atoms of Val50 occupy almost the same positions as in PR, and no close contacts are found between the side chain of Val50 and the aniline group of the inhibitor (Figure 9).

The catalytic triplet residues 25−27 showed very low rmsd values of 0.02−0.12 Å for comparison of main chain atoms, consistent with the uniquely conserved active site. Slightly larger differences in the positions of the catalytic triad are observed in PR_{L90M} structure, where the rmsd values are increased to 0.17−0.19 Å. Methionine is one methylene group longer than leucine. The side chain of residue 90 is located just underneath the catalytic residue Asp25 and therefore can directly influence the PR catalytic properties by making close interactions to the aspartate atoms. The wild type Leu90 has only van der Waals contacts with the main-chain atoms of Asp25, which are 3.7−4.0 Å long for both subunits. In contrast, in PR_{L90M} the long chain of Met90 protrudes further and its terminal methyl group (68% populated conformation) has very close contacts of 3.1−3.3 Å to the main-chain carbonyl of Asp25 (Figure 10), as reported for other complexes with L90M mutant.[20,24,31] The interactions are the same for the other subunit where residue 90′ has alternate conformations with 48/52% occupancy. Due to the repulsive nature of the above contacts the catalytic triads from both subunits shift slightly toward the inhibitor relative

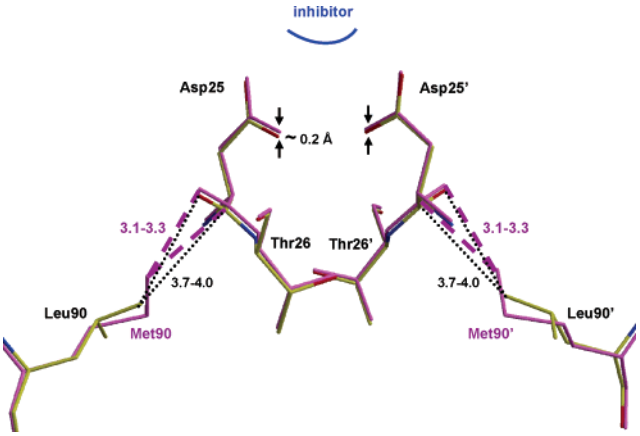

Figure 10. Interactions of mutated residues 90 and 90′ with catalytic residue 25 and 25′ shown in superimposed mutant and PR_{WT} structures. Interatomic distances are indicated by broken lines with the separation in Å. PR_{L90M} is shown in magenta bonds and PR in atom-type colored fashion. The side-chain conformations of Met90 and Met90′ that make shortened contacts to the main-chain atoms of aspartates are shown.

to their positions in the wild-type structure. Perhaps these highly unfavorable interactions are responsible for the diminished stability, which is reduced by ∼50% compared to the wild-type protease,[20] and slightly higher activity of the L90M mutant for the cleavage of the fluorescent substrate used in this study.

E. General Comparison of Interactions in TMC-114 and Indinavir Structures. It is instructive to compare the protease interactions of TMC-114 with those made by the clinical drug indinavir (IDV). Crystal structures with indinavir have been obtained for the wild-type PR−IDV and mutant proteases PR_{I50V}−IDV, PR_{V82A}−IDV, and PR_{L90M}−IDV.[20,32] The PR_{I50V}−IDV crystals diffracted to a very high resolution (1.10 Å), while the other three had the resolution of 1.25−1.40 Å, which is comparable to that obtained for the protease−TMC-114 crystals. The indinavir complexes showed the inhibitor in one orientation, except for PR_{I50V}−IDV, which had two orientations of IDV similar to the structures with TMC-114. It is noteworthy that the protease dimers showed very low rmsd values (<0.3 Å) if they were in the same space group, while values were bigger (∼0.6 Å) if the dimers were in two different space groups. The same trend was observed for the protease−TMC-114 structures.

As mentioned above, TMC-114 inhibitor was designed to increase the number of strong favorable interactions with the PR, especially with the main-chain atoms. Hydrogen bonds are the strongest interactions that play a major role in stabilizing inhibitor binding in the active site cleft. Moreover, direct hydrogen bonding to the PR residues is more favorable and conserved than water-mediated interactions. Both IDV and TMC-114 have the hydroxyethyl isostere as the central part of the molecule, which mimics the transition state of the proteolysis reaction. This OH group always forms strong hydrogen bonds to all four carboxylate oxygens of Asp25 and Asp25′. In protease−IDV structures, the inhibitor forms hydrogen bonds directly to residues Asp29 and Gly27. Additional hydrogen bonds are formed in PR_{I50V}−IDV and PR_{L90M}−IDV to the terminal group of Arg8. In protease−TMC-114 structures, the presence of the bis-THF group on one end and the NH_2 group on the other end of the molecule allows for additional H-bonds to Asp/Asn30. The important difference in the H-bond network is that the IDV complexes have only two H-bonds to the main chain carbonyl or amide atoms, while the TMC-114 complexes contain five or six such interactions. Obviously, the inhibitor−main chain contacts are much more conserved and less susceptible to mutations than the interactions with the side chains. In this context, therefore, the ability of TMC-114 to make many hydrogen-bond interactions with the main chain provides the basis of its superiority over other known inhibitors.

Hydrophobic interactions, although not as strong as hydrogen bonds, are important for an inhibitor binding. There is no clear correlation between the number of hydrophobic contacts between an inhibitor and protease and the inhibitor's ability to suppress the activity of the protease mutants. For instance, there are 95 interactions with distances < 4.0 Å found in the PR_{V82A}−IDV structure, while there are 96 interactions in the PR−IDV. Despite this, the K_i value increases 2-fold for the inhibition of the V82A mutant. On the other hand, the K_i value for TMC-114 increases three times for the V82A mutant, but as many as 12 contacts are lost by the inhibitor's major orientation in the PR_{V82A}−TMC-114 structure compared to PR-TMC-114.

Discussion

The design goal for TMC-114 has been to achieve superiority over the available clinical drugs in suppressing the proliferation of the HIV virus by making more favorable strong interactions with the PR residues, especially with the main chain atoms. Such interactions are probably less susceptible to resistant mutations than those with the side-chain atoms.

The bis-THF moiety of TMC-114 allows the formation of several hydrogen bonds with the main-chain atoms of Asp29 and Asp30. These interactions are very weak or absent for its closest analogue amprenavir, which contains only the single THF group. Moreover, the PR−IDV structures contain only two direct H-bonds to the PR main chain, while six such interactions are present in the wild type and mutant PR structures with TMC-114 inhibitor. Therefore, TMC-114 may better adapt to mutations than IDV, making it more difficult for the virus to select resistant mutations.

Inhibition data for PR_{D30N}, PR_{I50V}, and PR_{L90M} have shown, however, that TMC-114 does lose some affinity for the PR, especially in the case of D30N and I50V mutations. The relative K_i values are ∼30 and ∼9 for the two mutants, respectively (Table 1). In PR_{D30N}, the inhibitor has a water-mediated contact to the side chain of Asn30, while in PR a direct hydrogen bond is observed with one of the alternate conformations of Asp30. Given that other interactions in the two structures are very similar, the substitution of a direct contact by a water-mediated interaction may explain the increased K_i value for PR_{D30N} compared to the wild-type PR. On the other hand, there are more changes in the interactions between the inhibitor and the protease in the PR_{I50V} structure, though the K_i does not increase as much. Although the inhibitor's aniline group shifts considerably from its position observed in the other structures (Figure 7) and decreases its interactions with the main chain of Asp30, the H-bond to the side chain is shortened by ∼0.2 Å. Thus, the strength of the aniline-to-Asp30 interaction is probably not significantly affected. However, the inhibitor loses favorable hydrophobic interactions in one orientation with the side chain of Val50 (Figure 9A). Since hydrophobic contacts are weaker than hydrogen bonds, it may explain why the K_i value increases less for PR_{I50V} than for PR_{D30N}. Unexpectedly, the inhibitor is found to have higher potency against the common mutant PR_{L90M}. The K_i value was decreased by about 7-fold with respect to that of PR. According to the crystal structure, the major alternate conformations (60% occupancy) of Met90 and Met90′ have very close unfavorable interactions with the main-chain carbonyl of the active site Asp25 and 25′ (Figure 10), while only van der Waals interactions are present in the PR structure. These close contacts push the active site residues toward the

inhibitor by about 0.2 Å. Consequently, TMC-114 has ~10 more van der Waals interactions <4.0 Å in PR_{L90M} structure than in the PR structure. Therefore, the L90M mutation results in the reduction of the size of the active site cleft, leading to a tighter binding of the inhibitor. Since this mutation appears as a major resistant mutation on treatment with saquinavir or nelfinavir, it may be suggested that these drugs do not favor a tighter active site cavity, unlike TMC-114. Additionally, the L90M mutation appears as a minor mutation during the treatment with any of the clinical drugs and is always accompanied by the mutations in the active site cleft. Therefore, it may have an additional compensatory role in increasing PR activity on the natural substrates and/or decreasing dimer stability in the presence of an inhibitor.

The kinetic measurements have shown that PR_{D30N} is only 10% as active as the wild-type protease on the fluorescent substrate, while PR_{I50V} is 40% as active. On the other hand, the potency of TMC-114 was reduced by about 30 and 9-fold, respectively, for PR_{D30N} and PR_{I50V}. We therefore suggest that the mutations D30N and especially I50V may be selected by the virus for resistance to TMC-114. As a consequence, TMC-114 is not expected to be a good salvage therapy candidate for the people who fail the nelfinavir regimen due to the presence of the viral strains that contain the D30N mutation in the protease. In contrast, the L90M mutation is unlikely to emerge as a primary resistance mutation during the treatment with the inhibitor TMC-114, although L90M is obviously favorable for resistance in combination with other mutations. Similarly, V82A and I84V mutations had minor effects on the inhibition of TMC-114[15] and hence are expected to show resistance only in combination with other mutations.

Materials and Methods

Protein Preparation and Kinetic Measurements. The HIV-1 protease (Genbank HIVHXB2CG) clone was constructed with the substitutions Q7K, L33I, and L63I, to minimize the autoproteolysis of the protease, and C67A and C95A, to prevent cysteine-thiol oxidation.[33] PR templates with the appropriate oligonucleotide primers were used to introduce the D30N, I50V, and L90M mutations. All constructs were generated using the Quick-Change Mutagenesis protocol (Stratagene, La Jolla, CA) and verified by DNA sequencing. Proteins were prepared using the protocol described elsewhere.[33] Kinetic parameters were determined by fluorescence assay as described previously.[34] The substrate Ac-RE(Edans)SQNY*PIVRK(Dabcyl)R-CO-NH_2 was used. Protease (10 μL, final concentration of 7−12 nM) was mixed with 100 μL of PNF buffer (250mM phosphate buffer, pH = 5.6, containing 500 mM NaCl, 1 mM EDTA, 5 mM dithiothreitol, and 5% glycerol) and the mixture preincubated at 37 °C for 5 min. The reaction was started by adding 90 μL of substrate (final concentration of 2−40 μM), and the mixture was assayed over 5 min for the increase in fluorescence. Inhibition assays were performed in the same way, but the reaction mixture contained 2 μL of DMSO or inhibitor dissolved in DMSO. The inner filter effect was determined by measuring the fluorescence as a function of the concentration of RE (Edans), at the substrate concentration range used for the kinetic measurements. Data analysis was performed with the program SigmaPlot 8.0.2 (SPSS Inc., Chicago, IL). k_{cat} and K_m values were obtained by employing standard data-fitting techniques for a reaction obeying Michaelis−Menten kinetics. K_i values were calculated from the IC_{50} values estimated from a dose−response curve with the fluorescent assay using the equation $K_i = (IC_{50} - [E]/2)/(1 + [S]/K_m)$, where [E] and [S] are the protease and substrate concentrations, respectively.[35]

Crystallographic Analysis. The crystals of the PR mutants complexed with the inhibitor TMC-114 were grown by the hanging-drop vapor diffusion method using a 5:1 ratio of inhibitor to protein. Crystals of PR_{D30N} grew with a well solution containing NaOAc buffer (pH = 4.6), 1% DMSO, 0.5% dioxane, and 10% NaCl as a precipitating agent. PR_{I50V} crystals grew using well solution containing NaOAc buffer (pH = 4.8), 2% DMSO, 0.5% dioxane, and 10% NaCl. PR_{L90M} crystals grew using a well solution with NaOAc buffer (pH = 4.2) and 5% NaCl. Crystals were frozen with a cryoprotectant of 20−30% glycerol. X-ray diffraction data were collected on the SER−CAT beamline of the Advanced Photon Source, Argonne National Laboratory. Data were processed using HKL2000.[36] The structures were solved by molecular replacement using the CPP4i suite of programs.[37] The starting model for molecular replacement was the wild-type PR complex with TMC-114 (PDB code 1S6G),[15] which has the same space group as the new structures. The structures were refined using SHELX97[38] and refitted using the O 8.0[39] program. Alternate conformations were modeled for the inhibitor and protease residues when they were obvious in the electron density maps. The solvent was modeled with ~200 or more water molecules, some with partial occupancy. The identity of ions and other solvent molecules from the crystallization conditions was deduced on the basis of the shape and peak height of the $2F_o - F_c$ electron density, the potential hydrogen bond interactions and interatomic distances. The PR_{D30N} crystal structure was refined with two chloride anions, one sulfate anion, and 199 water molecules, including partial occupancy sites. PR_{I50V} structure included a sodium cation, two chloride anions, two acetate anions, a glycerol molecule, and 206 water molecules, including partial occupancy sites. PR_{L90M} structure was refined with a sodium cation, two chloride anions, two glycerol molecules, and 213 water molecule, including partial occupancy sites. Anisotropic *B* factors were refined for all atoms. Hydrogen atom positions were included in the last stage of refinement using all data after all other parameters including the disorder had been modeled. The mutant crystal structures were compared with the wild type structure by superimposing their main-chain atoms using an implementation of the algorithm previously described.[40] Figures were made using O[39] and MolScript.[41] The structures were deposited with PDB codes 2F80 for PRD_{30N}, 2F8G for PR_{I50V}, and 2F81 for PR_{L90M}.

Acknowledgment. I.T.W. and R.W.H. are Distinguished Cancer Scholars. Y.T. has a Molecular Basis of Disease Fellowship. We thank the staff at the SER-CAT beamline at the Advanced Photon Source, Argonne National Laboratory, for assistance during X-ray data collection. Use of the Advanced Photon Source was supported by the U. S. Department of Energy, Basic Energy Sciences, Office of Science, under Contract No. W-31-109-Eng-38. The research was supported in part by the Molecular Basis of Disease Program, the Georgia Research Alliance, the Georgia Cancer Coalition, the National Institute of Health grants GM62920, AIDS-FIRCA TW01001, and Hungarian OTKA F35191 and T43482.

References

(1) Barlett, J. A.; DeMasi, R.; Quinn, J.; Moxham, C.; Rousseau, F. Overview of the Effectiveness of Triple Combination Therapy in Antiretroviral-Naïve HIV-1 Infected Adults. *AIDS* **2001**, *15*, 1369−1377.

(2) Gulick, R. M.; Mellors, J. W.; Havlir, D.; Eron, J. J.; Meibohm, A.; Condra, J. H.; Valentine, F. T.; McMahon, D.; Gonzalez, C.; Jonas, L.; Emini, E. A.; Chodakewitz, J. A.; Isaacs, R.; Richman, D. D. 3-Year Suppression of HIV Viremia with Indinavir, Zidovudine, and Lamivudine. *Ann. Intern. Med.* **2000**, *133*, 35−39.

(3) De Clercq, E. New Approaches toward Anti-HIV Chemotherapy. *J. Med. Chem.* **2005**, *48*, 1−17.

(4) Wlodawer, A.; Vondrasek, J. Inhibitors of HIV-1 Protease: A Major Success of Structure-Assisted Drug Design. *Annu. Rev. Biophys. Biomol. Struct.* **1998**, *27*, 249−284. Wlodawer, A.; Gustchina, A. Structural and Biochemical Studies of Retroviral Proteases. *Biochim. Biophys. Acta* **2000**, *1477*, 16−34.

(5) Menedez-Arias, L. Targeting HIV: Antiretroviral Therapy and Development of Drug Resistance. *Trends Pharmacol. Sci.* **2002**, *23*, 381−388.

(6) Barbaro, G.; Scozzafava, A.; Mastrolorenzo, A.; Supuran, C. T. Highly Active Antiretroviral Tharepy: Current State of the Art, New Agents and Their Pharmacological Interactions Useful for Improving Therapeutic Outcome. *Curr. Pharm. Des.* **2005**, *11*, 1805−1844.
(7) Sax, P. E. Do New Protease Inhibitors Offer Improved Management Options? *J. AIDS* **2004**, *35*, S22−S34.
(8) Hertogs, K.; Bloor, S.; Kemp, S. D.; Van den Eynde, C.; Alcorn, T. M.; Pauwels, R.; Van Houtte, M.; Staszewski, S.; Miller, V.; Larder, B. A. Phenotypic and Genotypic Analysis of Clinical HIV-1 Isolates Reveals Extensive Protease Inhibitor Cross-Resistance: A Survey of Over 6000 Samples. *AIDS* **2000**, *14*, 1203−1210.
(9) Wu, T. D.; Schiffer, C. A.; Gonzales, M. J.; Taylor, J.; Kantor, R.; Chou, S.; Israelski, D.; Zolopa, A. R.; Fessel, W. J.; Shafer, R. W. Mutation Patterns and Structural Correlates in Human Immunodeficiency Virus Type 1 Protease Following Different Protease Inhibitor Treatments. *J. Virol.* **2003**, 4836−4847.
(10) Ohtaka, H.; Freire, E. Adaptive Inhibitors of the HIV-1 Protease. *Prog. Biophys. Mol. Biol.* **2005**, *88*, 193−208.
(11) Koh, Y.; Makata, H.; Maeda, K.; Ogata, H.; Bilcer, G.; Devasamudram, T.; Kincaid, J. F.; Boross, P.; Wang, Y.-F.; Tie, Y.; Volarath, P.; Gaddis, L.; Harrison, R. W.; Weber, I. T.; Ghosh, A. K.; Mitsuya, H. Novel bis-Tetrahydrofuranylurethane-Containing Nonpeptidic Protease Inhibitor (PI) TMC-114 (TMC-114) with Potent Activity against Multi-PI-Resistant Human Immunodeficiency Virus in Vitro. *Antimicrob. Agents Chemother.* **2003**, 3123−3129.
(12) Surleraux, D. L. N. G.; Tahri, A.; Verschueren, W. G.; Pille, G. M. E.; de Kock, H. A.; Jonckers, T. H. M.; Peeters, A.; De Meyer, S.; Azijn, H.; Pauwels, R.; de Bethune, M.-P.; King, N. M.; Prabu-Jeyabalan, M.; Schiffer, C. A.; Wigerinck, P. B. T. P. Discovery and Selection of TMC-114, a Next Generation HIV-1 Protease Inhibitor. *J. Med. Chem.* **2005**, *48*, 1813−1822.
(13) De Meyer, S.; Azijn, H.; Surleraux, D.; Jochmans, D.; Tahri, A.; Pauwels, R.; Wigerinck, P.; de Bethune, M.-P. TMC114, a Novel Human Immunodeficiency Virus Type 1 Protease Inhibitor Active against Protease Inhibitor-Resistant Viruses, Including a Broad Range of Clinical Isolates. *Antimicrob. Agents Chemother.* **2005**, 2314−2321.
(14) Shurtleff, A. C. TMC-114 (Tibotec). *Curr. Opin. Invest. Drugs* **2004**, *5*, 879−886. See also articles published on *clinialtrials.gov*.
(15) Tie, Y.; Boross, P. I.; Wang, Y.-F.; Gaddis, L.; Hussain, A. K.; Leshchenko, S.; Ghosh, A. K.; Louis, J. M.; Harrison, R. W.; Weber, I. T. High-Resolution Crystal Structures of HIV-1 Protease with a Potent Non-Peptide Inhibitor (TMC-114) Active against Multi-Drug-Resistant Clinical Strains. *J. Mol. Biol.* **2004**, *338*, 341−352.
(16) King, N. M.; Prabu-Jeyabalan, M.; Nalivaika, E. A.; Wigerinck, P.; de Bethune, M.-P.; Schiffer, C. A. Structural and Thermodynamic Basis for the Binding of TMC-114, a Next-Generation Human Immunodeficiency Virus Type 1 Protease Inhibitor. *J. Virol.* **2004**, 12012−12021.
(17) Velazquez-Campoy, A.; Kiso, Y.; Freire, E. The Binding Energetics of First and Second Generation HIV-1 Protease Inhibitors: Implications for Drug Design. *Arch. Biochim. Biophys.* **2001**, *390*, 169−175.
(18) Velazquez-Campoy, A.; Luque, I.; Freire, E. The Application of Thermodynamic Methods in Drug Design. *Thermochim. Acta* **2001**, *380*, 217−227.
(19) Clemente, J. C.; Moose, R. E.; Hemrajani, R.; Whitford, L. R. S.; Govindasamy, L.; Reutzel, R.; McKenna, R.; Agbandje-McKenna, M.; Goodenow, M. M.; Dunn, B. M. Comparing the Accumulation of Active- and Nonactive-Site Mutations in the HIV-1 Protease. *Biochemistry* **2004**, *43*, 12141−12151.
(20) Mahalingam, B.; Wang, Y.-F.; Boross, P. I.; Tozser, J.; Louis, J. M.; Harrison, R. W.; Weber, I. T. Crystal Structures of HIV Protease V82A and L90M Mutants Reveal Changes in the Indinavir-Binding Site. *Eur. J. Biochem.* **2004**, *271*, 1516−1524.
(21) Rhee, S.-Y.; Gonzales, M. J.; Kantor, R.; Betts, B. J.; Ravela, J.; Shafer, R. W. Human Immunodeficiency Virus Reverse Transcriptase and Protease Sequence Database. *Nucleic Acids Res.* **2003**, *31*, 298−303.
(22) Jarvis, B.; Faulds, D. Nelfinavir: A Review of Its Therapeutic Efficacy in HIV Infection. *Drugs* **1998**, *56*, 147−167.
(23) Mahalingam, B.; Louis, J. M.; Reed, C. C.; Adomat, J. M.; Krouse, J.; Wang, Y.-F.; Harrison, R. W.; Weber, I. T. Structural and Kinetic Analysis of Drug Resistant Mutants of HIV-1 Protease. *Eur. J. Biochem.* **1999**, *263*, 238−245.
(24) Mahalingam, B.; Louis, J. M.; Hung, J.; Harrison, R. W.; Weber, I. T. Structural Implications of Drug-Resistant Mutants of HIV-1 Protease: High-Resolution Crystal Structures of the Mutant Protease/Substrate Analogue Complexes. *Proteins* **2001**, *43*, 455−464.
(25) Tisdale, M.; Myers, R.; Randall, S.; Maguire, M.; Ait-Khaled, M.; Elston, R.; Snowden, W. Resistance of the HIV Protease Inhibitor Amprenavir in Vitro and in Clinical Studies. *Clin. Drug Invest.* **2000**, *20*, 267−285.
(26) Johnson, V. A.; Brun-Vezinet, F.; Clotet, B.; Conway, B.; D'Aquila, R. T.; Demeter, L. M.; Kuritzkes, D. R.; Pillay, D.; Schapiro, J. M.; Telenti, A.; Richman, D. D. Update of the Drug Resistance Mutations in HIV-1. *Top. HIV Med.* **2004**, *12*, 119−124.
(27) Lam, P. Y. S.; Jahdav, P. K.; Eyermann, C. J.; Hodge, C. N.; Ru, Y.; Bacheler, L. T.; Meek, J. L.; Otto, M. J.; Rayner, M. M.; Wong, Y. N.; Chang, C.-H.; Weber, P. C.; Jackson, D. A.; Sharpe, T. R.; Erickson-Viitanen, S. Rational Design of Potent, Bioavalable, Nonpeptide Cyclic Ureas as HIV Protease Inhibitors. *Science* **1994**, *263*, 380−384.
(28) Lam, P. Y. S.; Ru, Y.; Jahdav, P. K.; Aldrich, P. E.; DeLucca, G. V.; Eyermann, C. J.; Chang, C.-H.; Emmett, G.; Holler, E. R.; Daneker, W. F.; Li, L.; Confalone, P. N.; McHugh, R. J.; Han, Q.; Li, R.; Markwalder, J. A.; Seitz, S. P.; Sharpe, T. R.; Bacheler, L. T.; Rayner, M. M.; Klabe, R. M.; Shum, L.; Winslow, D. L.; Korhauser, D. M.; Jackson, D. A.; Erickson-Viitanen, S.; Hodge, C. N. Cyclic HIV Protease Inhibitors: Synthesis, Conformational Analysis, P2/P2′ Structure−Activity Relationship, and Molecular Recognition of Cyclic Ureas. *J. Med. Chem.* **1996**, *39*, 3514−3525.
(29) Hodge, C. N.; Aldrich, P. E.; Bacheler, L. T.; Chang, C. H.; Eyermann, C. J.; Garber, S.; Grubb, M.; Jackson, D. A.; Jadhav, P. K.; Korant, B.; Lam, P. Y.; Maurin, M. B.; Meek, J. L.; Otto, M. J.; Rayner, M. M.; Reid, C.; Sharpe, T. R.; Shum, L.; Winslow, D. L.; Erickson-Viitanen, S. Improved Cyclic Urea Inhibitors of the HIV-1 Protease: Synthesis, Potency, Resistance Profile, Human Pharmacokinetics and X-ray Crystal Structure of DMP450. *Chem. Biol.* **1996**, *3*, 301−314.
(30) Steiner, T. C−H···O Hydrogen Bonding in Crystals. *Crystallogr. Rev.* **1996**, *6*, 1−51; Wahl, M. C.; Sundaralingam, M. C−H···O Hydrogen Bonding in Biology. *Trends Biochem. Sci.* **1997**, *22*, 97−102.
(31) Hong, L.; Zhang, X. C.; Hartsuck, J. A.; Tang, J. Crystal Structure of an in vivo HIV-1 Protease Mutant in Complex with Saquinavir: Insight into the Mechanisms of Drug Resistance. *Protein Sci.* **2000**, *9*, 1898−1904.
(32) Liu, F.; Boross, P. I.; Wang, Y.-F.; Tozser, J.; Louis, J. M.; Harrison, R. W.; Weber, I. T. Kinetics, Dimer Stability, and High Resolution Crystal Structures of HIV-1 Protease Drug Resistant Variants L24I, I50V, and G73S. *J. Mol. Biol.* **2005**, *354*, 789−800.
(33) Louis J. M.; Clore, G. M.; Gronenborn, A. M. Autoprocessing of HIV-1 Protease Is Tightly Coupled to Protein Folding. *Nat. Struct. Biol.* **1999**, *6*, 868−875.
(34) Bagossi, P.; Kadas, J.; Miklossy, G.; Boross, P.; Weber, I. T.; Tozser, J. Development of a Microtiter Plate Fluorescent Assay for Inhibition Studies on the HTLV-1 and HIV-1 Proteinases. *J. Virol. Met.* **2004**, *119*, 87−93.
(35) Maibaum, J.; Rich, D. H. Inhibition of Porcine Pepsin by Two Substrate Analogues Containing Statine: The Effect of Histidine at the P2 Subsite on the Inhibition of Aspartic Proteinases. *J. Med. Chem.* **1988**, *31*, 625−629.
(36) Otwinowski, Z.; Minor, W. Processing of X-ray Diffraction Data in Oscillation Mode. *Met. Enzymol.* **1997**, *276*, 307−326.
(37) Collaborative Computational Project, Number 4. The CCP4 Suite: Programs for Protein Crystallography. *Acta Crystallogr. D* **1994**, *50*, 760−763; Potterton, E.; Briggs, P.; Turkenburg, M.; Dodson, E. A Graphical User Interface to the CCP4 Program Suite. *Acta Crystallogr. D* **2003**, *59*, 1131−1137.
(38) Sheldrick, G. M.; Schneider, T. R. High-Resolution Refinement. *Met. Enzymol.* **1997**, *277*, 319−343.
(39) Jones, T. A.; Zou, J. Y.; Cowan, S. W.; Kjeldgaard, M. Improved Methods for Building Protein Models in Electron Density Maps and the Location of Errors in These Models. *Acta Crystallogr. A* **1991**, *47*, 110−119.
(40) Ferro, D. R.; Hermans, J. A Different Best Rigid-Body Molecular Fit Routine. *Acta Crystallogr. A* **1977**, *33*, 345−347.
(41) Kraulis, P. J. MOLSCRIPT: A Program to Produce Both Detailed and Schematic Plots of Protein Structures. *J. Appl. Crystallogr.* **1991**, *24*, 946−950.

JM050943C